Effect of Ca^{2+} Ions on the Adhesion and Mechanical Properties of Adsorbed Layers of Human Osteopontin

Bruno Zappone,* Philipp J. Thurner,† Jonathan Adams,‡ Georg E. Fantner,§ and Paul K. Hansma‡

*Liquid Crystal Laboratory, Regional Laboratory and Center of Excellence for Functional Nanostructured Materials, Centro Nazionale delle Ricerche and Istituto Nazionale per la Fisica della Materia, Arcavacata di Rende (CS) 87036, Italy; †Bioengineering Science Research Group, University of Southampton, Southampton, United Kingdom; ‡Department of Physics, University of California, Santa Barbara, California; and §Department of Materials Science and Engineering, Massachusetts Institute of Technology, Cambridge, Massachusetts

ABSTRACT Using an atomic force microscope and a surface force apparatus, we measured the surface coverage, adhesion, and mechanical properties of layers of osteopontin (OPN), a phosphoprotein of the human bones, adsorbed on mica. OPN is believed to connect mineralized collagen fibrils of the bone in a matrix that dissipates energy, reducing the risk of fractures. Atomic force microscopy normal force measurements showed large adhesion and energy dissipation upon retraction of the tip, which were due to the breaking of the many OPN-OPN and OPN-mica bonds formed during tip-sample contact. The dissipated energy increased in the presence of Ca^{2+} ions due to the formation of additional OPN-OPN and OPN-mica salt bridges between negative charges. The forces measured by surface force apparatus between two macroscopic mica surfaces were mainly repulsive and became hysteretic only in the presence of Ca^{2+}: adsorbed layers underwent an irreversible compaction during compression due to the formation of long-lived calcium salt bridges. This provides an energy storage mechanism, which is complementary to energy dissipation and may be equally relevant to bone recovery after yield. The prevalence of one mechanism or the other appears to depend on the confinement geometry, adsorption protocol, and loading-unloading rates.

INTRODUCTION

Human bone tissue is composed mainly of a network of type I collagen fibrils (~45% of dry weight) longer than 1 μm, coated with nanocrystals of a mineral that resembles carbonate apatite or hydroxyapatite $Ca_{10}(PO_4)_6(OH)_2$ (~45% of dry weight) (1). Mineralized collagen fibrils have a typical diameter of ~100 μm and the average interfibrillar distance is of a few nm. It has long been recognized that mechanical properties of bones such as stiffness, hardness, and toughness derive from this mixed organic-inorganic nanostructure (1–3). Much less is known about the structure and function of the nonfibrillar organic fraction of bone (5–10% of dry weight). Recent studies (2,4–6) indicate that noncollagenous proteins of the bone matrix, in particular human osteopontin (OPN), may form an adhesive and connective interface between mineralized collagen fibers, improving the resistance of bone to fracture (i.e., toughness).

OPN is a phosphoprotein belonging to the family of small integrin binding ligand *N*-linked glycoproteins. It is believed to be unstructured and flexible with a contour length of ~100 nm (7). The molecular mass is 55 kDa and the primary sequence contains 298 amino acids (AA) (Table 1): 25% of the AA are acidic and ~19% of the AA are predicted to be posttranslationally modified with negatively charged groups, in particular, PO_3^- groups (phosphorylation) (Netphos 2.0 (8)). Basic AA constitute ~15% of the sequence. Therefore, the isoelectric point (IEP) of OPN is low, IEP = 4.6 (9), and the molecule bears a net negative charge at neutral pH.

The adhesive and cross-linking properties of OPN are strongly affected by divalent calcium ions (5), which abundantly bind to the protein (10). Bound Ca^{2+} ions can reverse the charge of the numerous negatively charged sites of the OPN molecule, which become potential binding sites for salt bridges with other acidic sites. Atomic force microscopy (AFM) experiments on layers of OPN adsorbed on mica have shown that the protein readily binds to this surface and forms a random network of weak intra- and intermolecular bonds (5). After binding of the proteins to a nanometric AFM probe during layer-probe contact, a long-ranged, nonmonotonic adhesive force is observed upon retraction of the probe from the surface (Fig. 1).

This force has been attributed to two main factors (11). First, separating the probe requires the rupture of many intra- and intermolecular bonds in the network as well as protein-surface bonds. These bonds are noncovalent and weak (~1 eV bond energy). The strength and range of the adhesive forces increase in the presence of Ca^{2+} due to the formation of additional salt bridges. Second, the bonds hide (or protect) portions of the proteins from the stretching imposed by the retraction. When bonds break, these portions are released in the solution, where they freely fluctuate. This creates an attractive entropic force, which resists the conformational restriction imposed by the stretching (11). When the external stress on the network is released, the network relaxes and some of the broken bonds can reform. By this mechanism, OPN is able to repeatedly dissipate large amounts of energy without creating macroscopic fractures in the network or gaps

Submitted April 23, 2008, and accepted for publication June 3, 2008.

Bruno Zappone and Philipp J. Thurner contributed equally to this work.

Address reprint requests to Bruno Zappone, E-mail: zappone@fis.unical.it.

Editor: Jane Clarke.

0006-3495/08/09/2939/12 $2.00

doi: 10.1529/biophysj.108.135889

TABLE 1 AA composition of human OPN containing 298 AA (7) and predicted posttranslational modifications (Netphos 2.0 (8), NetClyc 1.0 (32), NetOGlyc 3.1 (33), NetNGlyc 1.0 (34), NetGlycate 1.0 (35), and Sulfinator (39))

AA	Percentage
Acid (D, E)	25
Basic (K, R, H)	15
Polar (N, Q, S, Y)	25
Hydrophobic (F, I, L, M, V, W)	18
Cysteine	0
Presumably modified:	—
Phosphorylated*	13
Glycosylated*	5
Sulphated*	0.7

*The actual number of posttranslationally modified AA is not known.

between the surfaces (5). These adhesive and network-forming properties of OPN may be representative of a general mechanism acting at the nanoscale to improve the toughness and self-repairing capability of bone matrix.

In this work, we used AFM force spectroscopy and the surface force apparatus (SFA) to study layers of OPN adsorbed on negatively charged mica surfaces. Our goal was to investigate the effect of calcium ions on a), the adsorption of OPN, which is negatively charged, on equally charged surfaces; b), the adhesion between two surfaces coated with OPN layers; and c), the mechanical response of the adsorbed layers

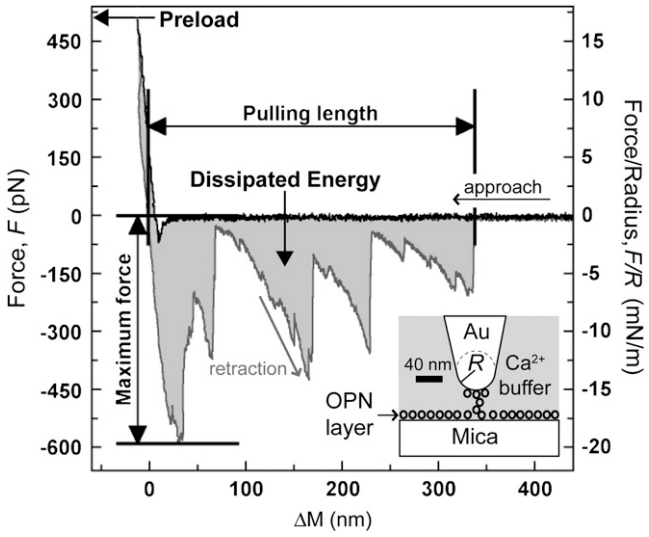

FIGURE 1 Typical force, F, obtained as a function of the scanner extension, ΔM, from AFM force spectroscopy measurements on mica surfaces bearing adsorbed OPN layers. In this example, the protein was adsorbed from a solution of 1:1 electrolyte inside the SFA then rinsed and studied in Ca^{2+} with the AFM. The vertical axis to the right shows the force F/R normalized by radius of curvature, $R \approx 30$ nm, of the Au-coated AFM tip. Notice the strong, long-ranged, and discontinuous attractive force measured upon retraction of the surfaces, which is due to the stretching of protein segments and the rupture of sacrificial bonds inside a protein network connecting the AFM tip to the surface. The figure also elucidates the parameters extracted from the force curve.

to repeated loading/unloading cycles. In the presence of calcium ions, OPN layers are plastically deformed during a compression/decompression cycle, likely due to the creation of numerous Ca^{2+}-mediated salt bridges during confinement. Only a fraction of these bonds is broken upon complete separation of the surfaces and most salt bridges appear to be permanent at the timescale of our experiment. Moreover, we have found that in general two OPN layers do not necessarily adhere to each other. As observed for other adhesive proteins (12), a strong adhesion is observed only when the OPN is allowed to adsorb simultaneously on two surfaces that are already in contact. These results provide more specific details about the proposed role of OPN as an adhesive in bone.

MATERIALS AND METHODS

OPN solutions, adsorption protocols, and buffers

Recombinant human OPN was prepared as described in Fedarko et al. (13). In a first set of AFM experiments, lyophilized OPN was dissolved at a concentration of 2 mg/ml in high performance liquid chromatography (HPLC)-grade purified water containing 0.02 M NaOH (pH = 12). OPN layers adsorbed from this solution were rinsed in one of the following buffers i), 150 mM NaCl, 10 mM HEPES, pH = 7.4; ii), 40 mM $CaCl_2$, 110 mM NaCl, 10 mM HEPES, pH = 7.4; or iii), 250 mM EDTA, a chelating agent for Ca^{2+} ions (pH = 8). In the following, we refer to solutions (i), (ii), and (iii), respectively, as NaCl, pure Ca^{2+}, and EDTA buffer (see also Table 2).

For SFA experiments, lyophilized OPN from the same purification batch was dissolved at a concentration of 0.2 mg/ml in HPLC-grade water containing 20 mM NaOH (pH = 12). This solution was stored in aliquots of ~50 μl at −18°C for <60 days before use. For the SFA experiments, a 25 μl droplet of this solution was inserted by capillarity between two cleaved ruby muscovite mica surfaces (S&J Trading, Glen Oaks, NY) and immediately supplemented with an equal volume of different buffers. The final solutions contained 0.1 mg/ml OPN dissolved in one of the following buffers: a), 10 mM NaOH; or b), 10 mM NaOH, 55 mM NaCl, 20 mM $CaCl_2$, 5 mM Tris. Both solutions had pH = 12. Adsorption proceeded in the sealed SFA box at 25°C for 1–2 h, during which the surfaces were either well separated at a large distance (>10 μm) or left undisturbed at adhesive mica-mica contact. After a first set of SFA measurements, the OPN-coated surfaces were rinsed in pure (OPN-free) electrolyte buffer containing c), 110 mM NaCl, 40 mM $CaCl_2$, and 10 mM TRIS at pH = 7.4. In the following, we will refer to solutions (*a*), (*b*), and (*c*), respectively, as OPN/NaOH, OPN/Ca^{2+}, and pure Ca^{2+} solution (see also Table 2).

TABLE 2 Measured parameters for OPN layers adsorbed on mica and studied in different buffers

Bulk solution	Γ (mg/m^2)	T_1 (nm)	A (mN/m)	d (nm)
OPN/NaOH*	2.4 ± 1.3	20	20	5
Rinsed with Ca^{2+}-buffer†	3.4 ± 1.2	30–40	306	2.2
Asymmetric in Ca^{2+}-buffer†	3.7 ± 1.5	15–20	65	1.6
OPN/Ca^{2+}‡	7.7 ± 1.2	30–45	171–502	4.5–8.4
Asymmetric in Ca^{2+}-buffer†	9 ± 2	50–60	—	—

Γ, surface coverage; T_1, uncompressed thickness; and A and d, parameters of the fit to the normalized force: $F/R = A\exp(-D/d)$.
*0.1 mg/ml OPN, pH ≈ 12.
†Tris buffer (10 mmol), NaCl (110 mmol), and $CaCl_2$ (40 mmol), pH ≈ 7.
‡0.1 mg/ml OPN in Tris buffer (5 mmol), NaCl (55 mmol), and $CaCl_2$ (20 mmol), pH ≈ 12.

After completing the SFA experiments, the mica surfaces coated with OPN from OPN/NaOH solution and rinsed in pure Ca^{2+} buffer were further studied by AFM in NaCl, pure Ca^{2+}, and EDTA buffers.

Surface force apparatus

The surface coverage, Γ, of OPN adsorbed on cleaved muscovite mica surfaces and the normal forces, F, between two such surfaces were measured using a surface forces apparatus (SFA, model SFA3), described in detail in Israelachvili and McGuiggan (14). Two back-silvered mica sheets were glued onto half-cylindrical glass lenses with a radius $R \approx 2$ cm using ultraviolet-curable polyurethane glue (NOA61 from Norland, Cranbury, NJ). The lenses were assembled in the SFA with the mica surfaces facing one another in a crossed-cylinder geometry. Around the point of closest approach (contact position), this geometry can be approximated to a sphere of radius R facing a flat surface (see *inset* of Fig. 3 *a*). The mica-mica separation distance, D, at the contact position was determined with subnanometer resolution by measuring the discrete set of interference fringes of equal chromatic order (FECO) selectively transmitted through the semireflecting silvered mica sheets (15). The position $D = 0$ was determined from the FECO fringes measured at mica-mica contact in dry air. A droplet of OPN solution was then inserted between the mica surfaces by capillarity.

To measure the normal force, F, acting between the two surfaces (see Fig. 3 *a*, *inset*), the lower surface was attached to a horizontal double cantilever spring of stiffness $K = 600$ N/m, which was displaced vertically toward or away from the upper surface with a motor-driven micrometer. As the surfaces were approached or retracted, the presence of an attractive or repulsive force caused the distance D to deviate from the values expected from a calibration of D versus the motor movement, which was made at distances >10 μm where $F = 0$. This deviation was due to the vertical deflection of the spring, which is proportional to F. A force curve was obtained by measuring F as a function of D upon approach then retraction of the surfaces while moving the lower surface by small steps. After each step, we waited and observed the FECO fringes to ascertain that the movement had stopped completely before measuring D to obtain an equilibrium (static) value of F. A typical SFA force run (approach or retraction) covered a mica-mica distance of $\sim$200 nm in 10–15 min. In view of Derjaguin approximation (16), the force F was normalized by the radius of curvature, R, determined for each experiment from the curved shape of the FECO fringes.

To determine the protein surface coverage, Γ, for each distance, D, we measured the combined refractive index, n, of the adsorbed protein layer and the bulk solution between the mica surfaces at the contact position. For a protein concentration, C, the refractive index is given by

$$n = n_w + C dn/dC, \quad (1)$$

where $dn/dC = 0.182$ cm^3/g is a typical value for proteins in electrolyte buffers of refractive index $n_w = 1.33$ (water) (17,18). For the small bulk concentration of OPN used in the SFA experiments, $C_{bulk} = 0.1$ mg/ml, a measurable increase of n from n_w was observed only for small values of D (see Fig. 3 *a*), when the volume fraction of proteins between the surfaces significantly increased due the presence of adsorbed OPN layers. In this case, the concentration of adsorbed molecules in the confinement was $C \approx p\Gamma/D$, where $p = 1$ or 2 depending on whether one or both surfaces were coated by OPN. Therefore, we determined Γ (in mg/mm^2) from a fit of the $n(D)$ curve to the following formula (19,20):

$$n(D) = n_w + p(\Gamma/D)dn/dC. \quad (2)$$

The normal force curves, $F(D)$, and refractive index curves, $n(D)$, were measured simultaneously. An example measurement is shown in Fig. 3 *a*.

For each contact position, we typically measured 2–3 force curves before moving to another contact position. On average 2–3 different contact positions were studied before changing the conditions of the experiment (surfaces or intervening medium). This typically took 1 day. To prevent evaporation of protein solutions during the experiments, the surfaces were sealed in a stainless steel box that contained a reservoir of water (not in direct contact with the surfaces). All experiments were carried out at a temperature of 25°C.

AFM force spectroscopy

We conducted two series of AFM force measurements on the same batch of OPN proteins. In the first series, we used a solution of 2 mg/ml OPN and 20 mM NaOH in purified water (pH = 12), as described above. A 4 μl droplet of solution was deposited on a freshly cleaved mica surface for $\sim$5 min, dried with N_2, and rehydrated in NaCl, pure Ca^{2+}, and EDTA buffers (see Fig. 2). In the second series, we used mica surfaces that had been previously coated from NaOH solution inside the SFA and used for a complete set of SFA measurements. The sample was kept hydrated with HPLC-grade water while mounting it onto the AFM scanner and, finally, completely immersed in pure-Ca^{2+} buffer. The AFM used for force spectroscopy measurements was a MultiMode system equipped with a PicoForce scanner, a Nanoscope IV controller, and a cell for measuring in liquids (Veeco, Santa Barbara, CA). We used a Biolever cantilever (model OBL-105, Olympus, Tokyo, Japan) bearing an Au-coated silicon tip with a final radius of curvature of $R \approx 30$ nm (Fig. 1, *inset*). The nominal cantilever stiffness was $K = 0.026$ N/m.

The AFM piezoelectric scanner was periodically moved in the vertical direction toward (approach) and away from (retraction) the AFM tip at a uniform speed of 900 nm/s. The scanner movement was reversed from approach to retraction when the tip-sample repulsive force exceeded a preload value of the force $F_p = 500$ pN, after a dwell time of 5 s (Fig. 1). This corresponded to $F_p/R \approx 17$ mN/m. The force always dropped to zero after completely separating the surface at a tip-sample distance larger than 1.5 μm (Fig. 1). We waited in this position for 5 s before starting a new approach/retraction cycle. For each mica surface, we considered an average of 25 positions on the surface and, for each position, an average of four force measurements.

RESULTS AND ANALYSIS

AFM force measurements

Fig. 1 shows an example AFM force curve obtained for a layer of OPN adsorbed on mica. The force, F, is plotted as a function of the AFM scanner movement, ΔM. Upon approach, the force became measurable at small tip-sample distances, where we observed a small attractive jump-to-contact with a jump-in distance of a few tens of nanometers. This was followed by a repulsive force ($F > 0$) that increased almost linearly when the distance was decreased and which was due to the compression and indentation of the AFM tip into the protein layer. The force measured during retraction of the scanner was very different from the one measured during approach. F became attractive ($F < 0$) at some value M_1 of the scanner position and remained attractive up to a certain position, $M_2 > M_1$, where it ultimately dropped to zero. We call pulling length the quantity $L = M_2 - M_1$ (Fig. 1).

Upon retraction, the attractive force decayed through a series of frequent, sharp discontinuities, passing through a maximum adhesion force F_m. This behavior was reproduced on successive approach/retraction cycles. The large hysteresis observed during an approach/retraction cycle is due to energy dissipation. We define the irreversible work done by the external force, F, during the ith cycle as $W_i = \oint F(D)dD$, where dD is the tip-sample displacement. In Fig. 1, W_i is approxi-

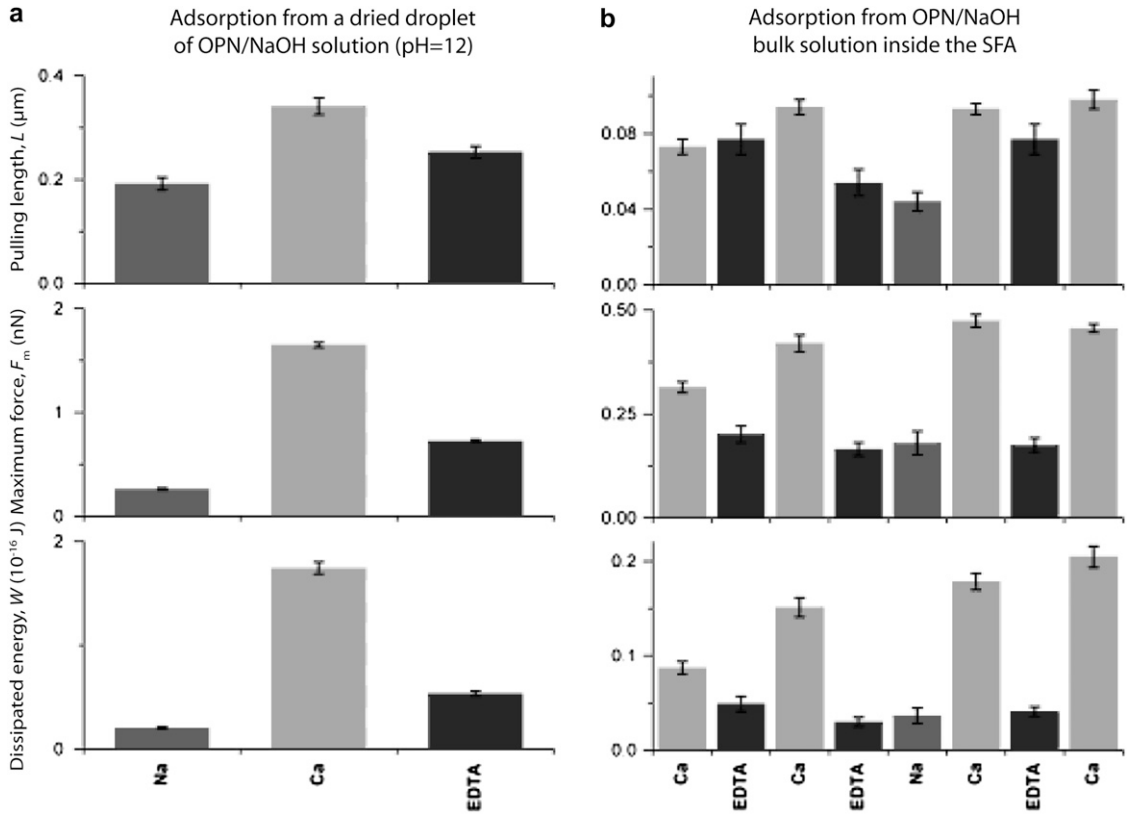

FIGURE 2 Summary of the AFM force spectroscopy results obtained after adsorption from 0.1–0.2 mg/ml solution of OPN/NaOH (pH = 12) on mica after two different adsorption procedures. The force measurements were carried out at pH = 7.4 after rinsing in OPN-free NaCl, $CaCl_2$, or EDTA buffers in the order specified in each panel. The values of the maximum pulling length, L, maximum adhesive force, F_m, and dissipated energy, W, have been averaged over ~100 force measurements. The error bars represent the standard error of the mean. Notice that W, F_m, and, less consistently, L increased when Ca^{2+} ions were present and decreased after chelating Ca^{2+} with EDTA. (*a*) Adsorption from a 4 μl droplet, which completely dried on the surface and was briefly rehydrated with purified water before the AFM measurements. (*b*) Adsorption inside the SFA box followed by a series of SFA force measurements (see Figs. 3 and 4) before AFM experiments. The surfaces were completely immersed in the OPN solution during adsorption and never dehydrated.

mately equal to the area between the approach and retraction parts of the force curve. In AFM force measurements, W_i randomly fluctuates around an average value, W, and the average value of the force during a cycle, f, was negative. Fig. 2 summarizes the values of L, F_m, and W, obtained for two different adsorption procedures. The results of Fig. 2 *a* were obtained from surfaces prepared directly for AFM measurements (dried droplet method), whereas Fig. 2 *b* was obtained from SFA samples. The samples were rinsed in a sequence of different buffers in the order specified in Fig. 2. The results obtained after each step were averaged over ~100 force measurements.

For OPN layers prepared with the dried droplet method, the value of L averaged over many pulls was larger than the contour length, $l_c \approx 100$ nm (7), of the OPN molecule, especially in the presence of calcium ions (Fig. 2 *a*). For OPN layers adsorbed inside the SFA, the average value was $L < l_c$, regardless of the presence of calcium ions (Fig. 2 *b*). However, for both adsorption methods, a certain number of pulls showed a value of L exceeding l_c up to four times. Clearly, proteins cross-linked in a network which adhered to the AFM tip and connected it to the mica surface. Proteins were stretched and bonds were broken upon retraction, generating the observed sequence of discontinuous force jumps (2,5,11). The averaged value of the energy W always increased when Ca^{2+} ions were present in the solution and decreased after chelating Ca^{+2} with EDTA, regardless of the adsorption conditions or the previous use of the surface in SFA experiments. L and F_{max} followed the same trend as W, although the results were less consistent.

The values of L, F_m, and W were about one order of magnitude higher for the AFM samples (dried droplet; Fig. 2 *a*) than for the SFA samples (Fig. 2 *b*). The SFA samples also showed a lesser repeatability of the force curves. Most likely, these differences were due to a higher surface coverage after adsorption from a drying droplet than after adsorption from bulk solution.

SFA force and surface coverage measurements

Fig. 3 *a* shows an example of a refractive index curve, measured after adsorption from OPN/NaOH solution for 1 h.

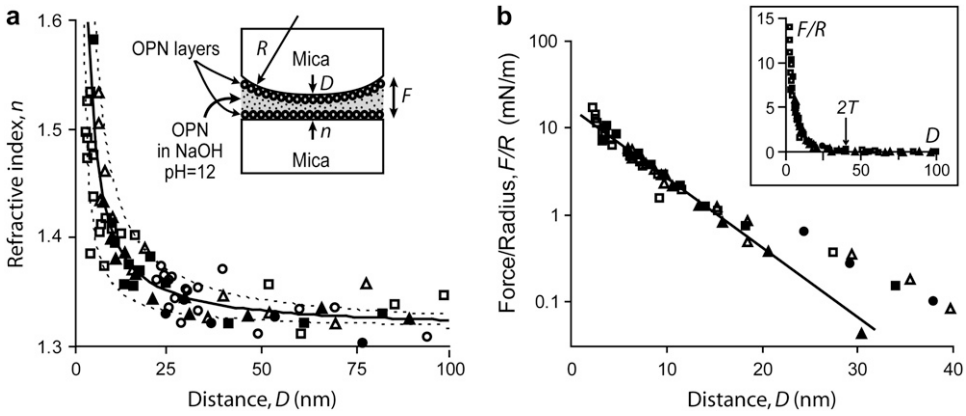

FIGURE 3 (*a*) Refractive index, n, as a function of the mica-mica distance, D, after adsorption from OPN/NaOH solution. Symbols (●/○), (■/□), and (▲/Δ) represent, respectively, the first, second, and third force runs at the same contact position. Solid/open symbols represent, respectively, approach and retraction of the surfaces. The solid line is a fit to Eq. 2 with $p = 2$ and a surface coverage $\Gamma = 2.4$ mg/m^2 (see also Table 2). The upper and lower dotted lines, corresponding respectively to surface coverage of 1.1 mg/m^2 and 3.7 mg/m^2, show the error on Γ due to the experimental error on n. (*Inset*) Geometry of the SFA experiment. R is the radius of curvature at the contact position and F is the normal force. (*b*) Semilog plot of the normalized force, F/R, as a function of D. (*Inset*) Linear plot for a larger scale. The force becomes measurable above the noise level of ~0.1 mN/m at a distance $D < 2T \approx 40$ nm. The solid line in the main panel is an exponential fit, $F/R = Ae^{-D/d}$, for $D < 20$ nm with $A = 20$ mN/m and $d = 5.0$ nm.

The refractive index, n, is plotted as a function of the mica-mica separation, D. The surfaces were approached then retracted three times at the same contact position, leaving them in contact from 1 to 30 min and well separated for 30 min to 1 h between consecutive contacts. The $n(D)$ curve was reproduced upon consecutive approach/retraction cycles indicating that 1), the surface coverage had reached equilibrium before the beginning of the measurements, and 2), the adsorbed layers were not squeezed out from the contact during compression (which would give a flat $n(D)$ curve (21)). The same behavior was observed in all SFA experiments. Table 1 is a summary of the surface coverage, Γ, measured in each experiment. We noticed that when the mica surfaces were kept in direct contact during adsorption from OPN/Ca^{2+}, the surface coverage in the mica-mica contact area was below the detection limit, $\Gamma < 1$ mg/m^2. The surface coverage remained undetectable even after keeping the surfaces well separated in OPN/Ca^{2+} solution for more than 30 min, indicating that no further adsorption occurred.

Adsorption from OPN/NaOH solution

After adsorption from OPN/NaOH solution, the surface coverage was $\Gamma = (2.4 \pm 1.3)$ mg/m^2 (Fig. 3 *a* and Table 1). Fig. 3 *b* shows the normal forces, F, normalized by the radius of curvature R of the crossed SFA cylinders, corresponding to the refractive index curve of Fig. 3 *a*. The force was reproducible and repulsive, without any indication of adhesion or hysteresis during an approach/retraction cycle, regardless of the maximum compression force applied or the dwelling time in contact. The range of the repulsion, defined as the maximum distance at which the force raises above the noise level of ~0.1 mN/m, was $2T \approx 40$ nm. This value is much longer than the value of the Debye length, $1/\kappa \approx 3$ nm, expected for the electrostatic double-layer repulsion between two negatively charged surfaces interacting across the NaOH solution (16). Therefore, the repulsive force was due to the partial overlap and deformation of the adsorbed OPN layers for distances $D < 2T$. Since the two mica surfaces are equally coated by OPN, we conclude that $T \approx 20$ nm is the thickness of one adsorbed OPN layer (see also Table 2). For distances $D < 20$ nm, the repulsion was almost exponential, $F/R = A\exp(-D/d)$ (Fig. 3 *b*), with a decay length $d = 5.5$ nm and amplitude $A = 20$ mN/m (Table 2). The force decayed less rapidly for larger distances.

Rinsing with Ca^{2+} buffer

After rinsing the surfaces with pure Ca^{2+} buffer inside the SFA without changing the contact position, the surface coverage increased to $\Gamma = (3.4 \pm 1.2)$ mg/m^2, which is ~42% higher than the value measured in OPN/NaOH solution before rinsing (Table 2). Also the range of the repulsion measured upon the first approach was increased by ~50% to $2T_1 \approx 60$ nm (Fig. 4, *a* and *b*, and Table 2). Since the Ca^{2+} buffer had a higher ionic strength (total concentration of counterions) than the OPN/NaOH solution and a shorter Debye length $1/\kappa < 3$ nm (16), the increase of the repulsive range can be due only to an increased thickness of the adsorbed OPN layers. The larger values of T_1 and Γ measured after rinsing clearly indicate that new OPN molecules were added to the layers due to Ca^{2+}-activated bonds.

The force curve showed a large hysteresis during an approach/retraction cycle. The average value of the force during a cycle, f, was positive. The irreversible work, $W_i = \oint F(D)dD$, done by the external forces during the ith cycle (Fig. 4 *b*) decreased with the number of successive approach-retraction cycles done at the same contact location. W_i was

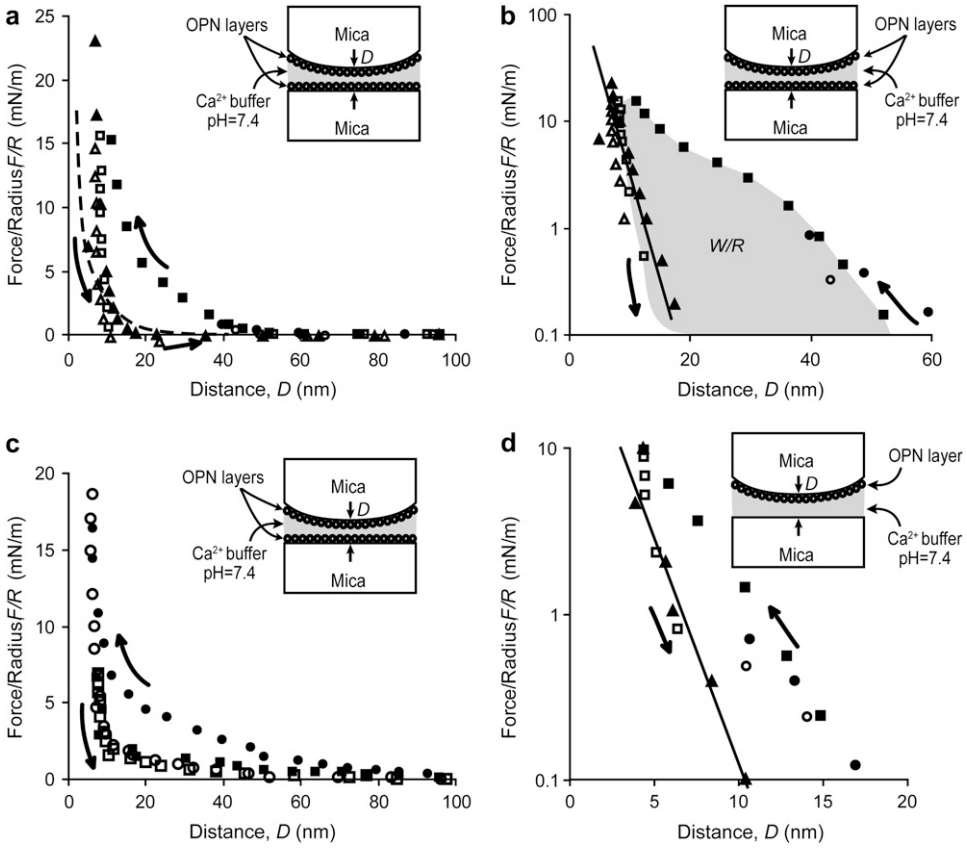

FIGURE 4 Normalized force, F/R, measured as a function of the mica-mica distance, D, for the same surfaces as in Fig. 3 after rinsing with pure Ca^{2+} buffer. In all panels, solid/open symbols represent, respectively, approach/retraction of the surfaces, and the symbols (●/○), (■/□), and (▲/Δ) represent, respectively, the first, second, and third cycles. (*a*) Force measured at the same contact position as in Fig. 3. Notice the large hysteresis measured for the second approach/retraction. The arrow at $D \approx 22$ nm is a jump-out from a shallow adhesive minimum. The dashed line represents the data of Fig. 3 *b*. (*b*) Semilog plot of the same figure. The solid line is an exponential fit, $F/R = Ae^{-D/d}$, with $A = 306$ mN/m and $d = 2.2$ nm. The shaded area between is proportional to the work, W, done by the external forces during the second cycle. (*c*) Force measured at a new contact position where surfaces have not been in contact before. (*d*) Force measured in the asymmetric configuration obtained after replacing the upper surface with an uncoated mica surface. The solid line is an exponential fit, $F/R = Ae^{-D/d}$, for $D <$ 20 nm with $A = 65$ mN/m and $d = 1.6$ nm.

large when the maximum force (preload), F_p, reached a high value during loading. For example, the value of W_1 obtained for $F_p/R < 1$ mN/m in Fig. 4 *b* (*circles* and *dots*) was smaller than the value of W_2 obtained for $F_p/R > 10$ mN/m (Fig. 4 *b*, *squares*). The hysteresis rapidly decreased with the number of cycles, so that the total work done, $W_{tot} = \sum W_i$, tended to a finite value. The range of the repulsion was also rapidly reduced after a few cycles with high F_p and tended to a value $2T \approx 20$ nm, less than half the initial value $2T_1$. The force became approximately exponential for $D < 20$ nm: $F/R = Ae^{-D/d}$ (Fig. 4 *b*). The decay length, $d = 2.2$ nm, was smaller than before rinsing, but the amplitude $A = 306$ mN/m was much larger (Table 2). A weak adhesive force with $-F/R \ll 1$ mN/m was also observed for this contact position. The attractive region extended from $D_m \approx 12$ nm to a distance of ≈23 nm, where a jump-out was observed toward a region of zero force.

We obtained similar results at different contact positions (Fig. 4 *c*) where surfaces had never been in contact before. The repulsion measured upon the first approach was always in the range $2T_1 = 60$–80 nm and reduced to $2T = 30$–40 nm after a few cycles with high preload. However, the force did not always tend to a simple exponential at short distances, and the weak adhesive minimum was not detected at each contact position (Fig. 4 *c*). This nonreproducibility is confirmed by later AFM measurements on the same surfaces (Fig. 2 *b*) and indicates a heterogeneity of the OPN layers after rinsing with Ca^{2+} buffer.

We obtained an asymmetric OPN/mica contact by replacing one of the surfaces with a bare (uncoated) mica surface (Fig. 4 *d*). The surface coverage Γ was about half the value measured for two symmetrically coated mica surfaces (Table 2). The normal forces were again purely repulsive, with an initial repulsion range $T_1 = 15$–20 nm, equal to the thickness of one layer. We notice that $2T_1 \approx 30$–40 nm is smaller than the value of 30–40 nm measured for one layer in the symmetrical case, possibly due to previous accidental contact at the same position. The range of the repulsion after a few cycles reduced to $T \approx 10$ nm. We notice again that the value of W_i measured during cycles with low preload $F_p/R <$ 1 mN/m (Fig. 4 *d*, *dots*) was much smaller than the value measured upon the second cycle (Fig. 4 *d*, *squares*). The final force was roughly exponential for $D < 10$ nm, with a decay length $d = 1.6$ nm and an amplitude $A = 65$ mN/m (Fig. 4 *d*) (Table 2).

Adsorption from OPN/Ca^{2+} solution

After adsorption from OPN/Ca^{2+} solution, the surface coverage was $\Gamma \approx (7.7 \pm 1.2)$ mg/m^2, which is ~3 times higher than the value measured after adsorption from OPN/NaOH solution (before rinsing) (Table 2). The force curves, $F(D)$, were purely repulsive and showed a large hysteresis (Fig. 5, *a* and *b*), which was similar to the one described for an OPN layer adsorbed from OPN/NaOH solution and rinsed in Ca^{2+}

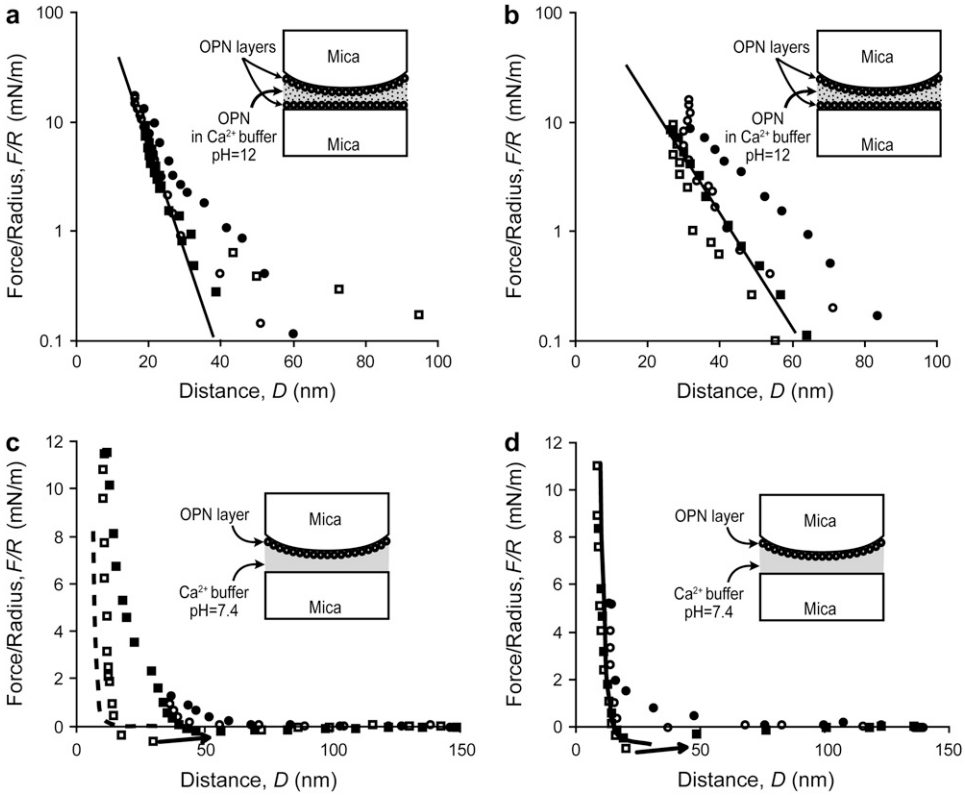

FIGURE 5 Normalized force, F/R, as a function of the mica-mica distance, D, after adsorption from OPN/Ca^{2+} solution. Solid/open symbols represent data obtained upon approach/retraction of the surfaces. The symbols (●/○) and (■/□) indicate, respectively, the first and second approach/retraction cycles at the same contact position. (*a*) The solid line is an exponential fit, $F/R = Ae^{-D/d}$, for $D < 30$ nm with $A = 502$ mN/m and $d = 4.5$ nm. (*b*) A new contact position, where $A = 171$ mN/m and $d = 8.4$ nm. (*c*) Force measured after rinsing the surfaces in Ca^{2+} buffer (pH = 7.4) and replacing one surface with a bare (uncoated) mica surface. The dashed line represent the data of Fig. 4 *d*. (*d*) A new contact position. The solid line represent the last retraction of *c*. The arrows for $F < 0$ in *c* and *d* indicate jumps-out from adhesive minima.

buffer (Fig. 4, *a–c*). Again, the total irreversible work, W_{tot}, done by the external forces rapidly tended to a finite value after a few approach/retraction cycles with high preload. The initial range of the repulsion was $2T_1 \approx 60$–90 nm and reduced by ~30% to a final value of $2T \approx 40$–60 nm (~30%). The force became approximately exponential for $D < 40$ nm, $F/R = Ae^{-D/d}$, with a decay length $d = 4.5$–8.4 nm and an amplitude $A = 170$–501 mN/m (Table 2). Both values were larger than those measured after adsorption from OPN/NaOH before rinsing. We noticed that the values of d and A showed a large dispersion, indicating a nonuniformity of the adsorbed layers.

In the asymmetric configuration (Fig. 5, *c* and *d*), Γ remained comparable to the value measured before rinsing (Table 2), indicating that there was no significant desorption. The force measured upon the first approach was purely repulsive, with a range $T_1 \approx 50$–60 nm. The range of the repulsion was reduced by ~78% after a few cycles and the final value was $T \approx 15$ nm (Fig. 5 *c*), which is about half the final value measured for symmetrically coated surfaces (Fig. 5, *a* and *b*). After a few approach/retraction cycles, we consistently observed a small attractive force upon retraction, reaching a maximum adhesion force $F_m/R = 0.3$–1 mN/m (Fig. 5, *c* and *d*). The attraction started at a distance $D_{min} = 20$–30 nm and was measurable over a range $L_{SFA} = 10$–20 nm (Fig. 5 *c*). L_{SFA} appeared to decrease after a few approach/retraction cycles (Fig. 5 *d*). A very weak attraction was also observed during approach and is visible in Fig. 5, *c* and *d*, as a negative background for the repulsion at a distance between 50 nm and 100 nm, possibly leading to a jump-to-contact from 50 nm to $D \approx D_{min}$. We notice that the asymmetrical configuration and the Ca^{2+} buffer considered here are the same as considered in Fig. 4 *d*, where the protein was first adsorbed from OPN/NaOH solution then rinsed in Ca^{2+} buffer. However, in the latter case no adhesion was observed.

The importance of adsorption conditions in determining adhesion is further evidenced in Fig. 6, where proteins were adsorbed from OPN/Ca^{2+} solution as for Fig. 5 but on mica surfaces that were kept in contact ($D = 0$) during adsorption. First, we measured the adhesion between the bare mica surfaces in pure Ca^{2+} buffer (before introducing the OPN solution), which was $F/R = -45$ mN/m. Then, we added a droplet of protein solution while keeping the mica surfaces in contact (Fig. 6). The adhesion measured during the first retraction after 2 h of adsorption was $F/R \approx -220$ mN/m, significantly stronger than between bare mica surfaces and one order of magnitude higher than typical values measured in the AFM experiments in the presence of Ca^{2+} (Fig. 1 and (5)). The adhesion rapidly decreased after the first retraction in OPN/Ca^{2+} solution. During retraction, the distance did not significantly deviate from D_m until the surfaces separated with a single, rapid jump-out from D_m to a distance larger than the contour length, $l_c \approx 100$ nm, of the OPN molecule. After 12 h of repeated approaches and retractions, the force became purely repulsive with a range not exceeding a few nanometers.

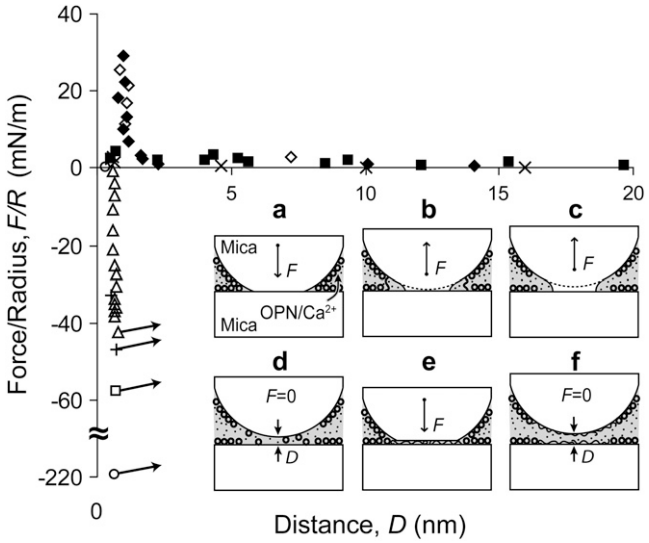

FIGURE 6 Normalized force, F/R, as a function of the distance D between two mica surfaces that were held in contact during adsorption from OPN/Ca^{2+} solution. Solid/open symbols indicate approach/retraction of the surfaces. Symbols (○) represent the first retraction, and symbols (■/□), (▲/Δ), and (◆/◇) represent, respectively, the second, fifth and seventh approach/retraction cycles, which followed the first retraction by 30 min, 2 h, and 16 h. Symbols ×/+: forces measured upon approach/retraction in pure Ca^{2+} between uncoated mica surfaces before injecting any OPN solution. The surfaces adhere upon retraction until they suddenly jump apart to separations $D > 200$ nm from the points indicated by the arrows. (*Inset*) (*a*) Proteins adsorb at the edge of the mica-mica contact region; (*b*) protein bridges at the edge of this region are stretched; and (*c*) broken during the first retraction whereas mica surfaces remain in contact; (*d*) incomplete adsorption in the contact area after mica-mica separation; (*e*) flattening during second approach; (*f*) protein remains flattened after the surfaces are separated again.

DISCUSSION

Solutions of 1:1 electrolytes

At the neutral and basic pH of our experiments, OPN bears a net negative charge (IEP = 4.6; (9)) due to its numerous negatively charged residues (Table 1). Mica is also negatively charged due to the dissociation of K^+ ions from the surface in water (22). Although the overall OPN-mica electrostatic interaction is repulsive, OPN adsorbs on mica from OPN/NaOH solution, forming a layer with a thickness $T \approx 20$ nm (Table 2 and Fig. 3 *b*) and a surface coverage $\Gamma = 2.4$ mg/m^2 (Table 2) corresponding to an average lateral distance $s = (M_w/N_A\Gamma)^{1/2} = 6$ nm. Adsorption of charged proteins (23–26) and polymers (27) on equally charged surfaces has been previously reported and is driven by a combination of factors.

First, OPN is an unstructured protein (7), and it is flexible. If it was uncharged, it would form random coils in solution with a radius of gyration given by Flory's formula (28): $G_0 \sim aN^{3/5} \sim 10$ nm, where $N = 298$ is the number of AA and $a = 0.4$ nm is the average distance between neighboring AA. The electrostatic repulsion between negatively charged AA belonging to the same protein tends to stiffen the molecule and swell the coil to a diameter $2G > 2G_0$. However, this effect is partially balanced by the presence of counterions in our solutions (Table 2), which can neutralize the negative charges and reduce the Debye length to a few nanometers (16). Since SFA experiments show that s is smaller than both T and $2G$, we conclude that in our solution OPN is rather flexible and deforms considerably on the surface in response to interactions with the surface and with other proteins. We notice that both s and $2G$ are smaller than the protein contour length $l_c = aN \approx 100$ nm (7).

Second, OPN is amphoteric and contains positively charged residues and uncharged polar AA with high affinity for the negatively charged and polar sites on the mica surface. At the relative concentration $\log_{10}([Na^+]/[H^+]) > 5$ of our OPN/NaOH solution, most of the negatively charged lattice sites of the mica surface are neutralized by Na^+ (29) and the overall OPN-mica repulsion is weak and short ranged. Binding of surface-active AA is strong enough to immobilize the protein despite the repulsive background. This mechanism—also known as electrostatic complementarity (30)—is effective for deformable proteins with mobile AA: isolated residues can be anchored on the surface, whereas nonbinding residue can be repelled or left free in the solution. The OPN layers adsorbed from OPN/NaOH solution preferentially expose negatively charged residues at the free surface of the layer, which repel equally charged residues belonging to an opposite surface. The force F between two OPN layers is therefore repulsive. F becomes approximately exponential at sufficiently small values of the mica-mica distance ($D < 20$ nm, Fig. 3 *b*). This behavior is frequently observed for flexible, charged biopolymers on equally charged surfaces (24–26) and is generally attributed to electroentropic interactions (see Leckband and Israelachvili (30) and Claesson et al. (31) for reviews). These are due to the combination of protein-protein, intraprotein, and surface-protein electrostatic repulsion between equally charged sites and entropic-osmotic forces, which arises when the molecules are confined in a geometry restricting their conformational freedom.

Third, the overall OPN-OPN electrostatic interaction is always repulsive, but its strength and range are reduced in the presence of counterions. This results in a higher density of coadsorption and also allows isolated cross-links to effectively stabilize aggregates against the background repulsion. This effect was observed in AFM force measurements on OPN layers adsorbed with the dried droplet method (Fig. 2 *a*, *first row*) before contact with Ca^{2+} ions. The average value of L was twice as long as the contour length l_c of a single OPN molecule. We also notice that the concentration, ρ, of proteins in the adsorbed layers was orders of magnitude higher than the concentration in solution. For example, OPN layers adsorbed in the SFA from OPN/NaOH solution showed a relatively small surface coverage, Γ (Table 2), and layer thickness, T (Fig. 3 *b*), and yet the concentration inside the adsorbed layer was $\rho = \Gamma/T \approx 120$ mg/ml. This is three orders of magnitude larger than the concentration $C = 0.1$ mg/ml of

the bulk solution. After the adsorption procedure used in the AFM experiments of Fig. 2 *a* (drying droplet method), ρ is expected to be even higher than the value calculated above. This high value of ρ dramatically increases the density of binding pairs and the probability of cross-linking inside the layer. On the other hand, it is likely that cross-links form at low rates and/or densities between two OPN layers that are compressed on each other during an SFA measurement, as no adhesion could be detected upon retraction in these measurements (Fig. 3 *b*).

Although the precise nature of OPN cross-links in the absence of calcium is not clear, we may speculate that bonds are formed between oppositely charged residues or between hydrophobic AA. Moreover, molecules can be physically entangled inside the layer without being bound to each other, especially after adsorption with the dried droplet method used for the AFM samples.

Effect of divalent counterions: energy storage and dissipation

Ca^{2+} ions can bind to and reverse the sign of negative charges on the mica surface and OPN molecules. Mica is negatively charged in $CaCl_2$ solutions up to a concentration of 100 mM (31). For the lower $CaCl_2$ concentrations of our solutions (Table 2), where Ca^{2+} had to bind to mica in competition with monovalent counterions, mica is expected to retain a net negative charge. OPN has a significant calcium-binding potential due to the high level of phosphorylation. In a solution containing 5 mM $CaCl_2$ and 150 mM NaCl at pH > IEP, ~50 AA can be charge-reversed (10), corresponding to ~38% of the predicted number of negatively charged residues (Netphos 2.0 (8), NetClyc 1.0 (32), NetOGlyc 3.1 (33), NetNGlyc 1.0 (R. Gupta, E. Jung, and S. Brunak, unpublished), and NetGlycate 1.0 (35)). We expect more Ca^{2+} ions to be bound to OPN in our solutions, where the concentrations of $CaCl_2$ were, respectively, four and eight times higher than in Chen et al. (10) (Table 2).

Binding of Ca^{2+} reduced the overall electrostatic OPN-OPN and OPN-mica repulsion, so that isolated bonds and salt bridges were more effective in cross-linking and binding the proteins to the surface. The surface coverage, Γ, and the thickness of an uncompressed layer, T_1, were higher than the values measured in the absence of Ca^{2+} (Table 2). The increase was particularly informative when OPN layers adsorbed from and immersed in a basic solution of 1:1 electrolytes (Fig. 3) were rinsed with OPN-free Ca^{2+} buffer (Fig. 4, *a–c*). In this case, we expected the surface coverage to remain constant or decrease because the dilution of the bulk protein concentration and the shearing action of the buffer flow usually remove molecules from the adsorbed layer. However, Ca^{2+} activated new salt bridges between negatively charged sites and these bonds were numerous and strong enough to immobilize more proteins on the surface against the very flow that supplies the Ca^{2+} ions.

Calcium-mediated bonds were created and broken under the effect of an externally applied stress in such a way that the OPN layers behaved inelastically. Both AFM and SFA force measurements showed an increased hysteresis during an approach/retraction cycle in the presence of Ca^{2+} ions. In AFM experiments, the average force, f, in a cycle is negative (Fig. 1), and the irreversible work done fluctuates around a constant average, W, as the number of cycles increases (Fig. 2). This behavior is consistent with an energy dissipation mechanism (5,11) that begins when a few proteins bind to the AFM probe during contact with the adsorbed OPN layer. Upon retraction of the probe, these proteins are directly stretched, but they also indirectly stretch other adsorbed proteins or portions of proteins to which they may be attached. The stretching is resisted by an entropic force, resulting in the long-ranged, discontinuous, large adhesion observed in AFM force measurements (Fig. 1). Discontinuities in the adhesive force are interpreted as rupture events occurring when intraprotein, protein-protein, or surface-protein bonds are broken under the effect of excessive stretching. The rupture of these sacrificial bonds redistributes the force onto other parts of the network which were previously hidden by the sacrificial bond. The subsequent stretching against the entropic elasticity of this hidden length makes the largest part of the energy, W, dissipated in a cycle (11). The increase of W in the presence of Ca^{2+} is due to the creation of additional Ca^{2+}-mediated bonds which shield more hidden length, whereas the reduction of W after chelation with EDTA (Fig. 2) is due to the removal of these bonds. Notice that this mechanism is based on cross-layer bonds formed between proteins of the OPN layer and the opposing surface, as opposed to intralayer bonds formed between proteins belonging to the same layer or between these proteins and the underlying mica surface. In fact, cross-layer bonds create adhesion ($f < 0$) when stretched and must all be broken to completely separate the surfaces. Upon successive contacts, they can be reformed to obtain similar adhesion and energy dissipation, W.

In SFA experiments (Figs. 4 and 5), the work W_i done in a cycle progressively decreases as the number of cycles at the same contact location increases. After a few cycles, the total work, $W_{tot} = \sum W_i$, tends to a finite value. Adhesion is never observed upon the first retraction, and the average force, f, in a cycle is always positive. We interpret this behavior as an energy storage mechanism in which a maximum amount of energy, W_{tot}, can be stored in the adsorbed layer(s) upon compression. The fact that W is measurable only in the presence of Ca^{2+} indicates that the energy is stored in the form of long-lived Ca^{2+}-mediated bonds, which are created during compression due to the increased density of binding pairs. These bonds are mainly of the intralayer type and cause a compaction of the OPN layer. Cross-layer bonds are too weak or too few to generate a net adhesion or to break the intralayer bonds during retraction. As a result, the number of intralayer bonds rapidly reaches saturation, and the storage

mechanism stalls. Preliminary SFA force measurement between OPN-coated and gold-coated mica surfaces showed no significant deviation from this behavior, suggesting that the surface chemistry of the Au-coated AFM tip does not favor the adhesion of OPN and the creation of cross-layer bonds.

The energy dissipation mechanism via rupture of Ca^{2+}-mediated bonds observed by AFM has been proposed to explain the great toughness of bone, where a network of noncollagenous proteins including OPN is believed to reduce the creation and propagation of macroscopic fractures between bundles of mineralized collagen fibrils (2,4,6). The complementary energy storage mechanism that we observed by SFA may be equally important in real bones. Bond reformation upon compression of the noncollagenous protein matrix may help recover the fracture toughness after a prolonged tensile stress. We point out that the hysteresis and inelastic behavior shown by OPN layers during loading-unloading cycles are nonequilibrium phenomena—a situation common for charged polymers and biopolymers (27) and, in general, related to the inherently dynamic (nonstatic) nature of biological processes (30). On the timescale of our AFM and SFA experiments, Ca^{2+} salt bridges form and disappear very slowly, so that the number of bridges inside an OPN layer never stabilizes to the equilibrium value corresponding to instantaneous confinement conditions. Consider, for example, the limit condition of zero (noise-level) force, for which we estimated the layer thickness, T (*inset* of Fig. 3 *b*), from SFA measurements. A layer that has been previously compressed appears permanently compacted, i.e., it contains an excess of calcium bridges compared to an uncompressed (possibly equilibrium) layer. On the timescale of our experiments, this excess does not disappear when compression is removed: the layer is trapped in a nonequilibrium state.

From our SFA experiments, we could not determine the type of interaction that produces compaction, i.e., whether it is due to OPN-OPN or OPN-mica intralayer bonds. We cannot exclude the possibility that more than 50% of the negatively charged residues were bound by Ca^{2+}, so that the charge of OPN molecules became positive (most of the basic AA of the protein are neutralized by OH^- and negative counterions at the pH > IEP and salinity of our solutions) and the overall electrostatic OPN-mica interaction was reversed from repulsive to attractive. In fact, heavily charged cationic polyelectrolytes such as polylysine are known to strongly bind to mica in a nonequilibrium conformation that can be compacted by compression with a SFA (19). As for attractive cross-layer bonds, a net adhesion was consistently measured by SFA only between an OPN layer adsorbed from OPN/Ca^{2+} solution and rinsed in pure Ca^{2+} buffer and a bare mica surface (Fig. 5, *c* and *d*). This seems to confirm that the OPN-mica interaction is more attractive than the OPN-OPN interaction. On the other hand, under the same asymmetrical geometry and buffer conditions, a layer adsorbed from OPN/NaOH solution and rinsed in Ca^{2+} buffer did not show any adhesion (Fig. 4 *d*). Moreover, a small adhesion is occasionally detected between two mica surfaces equally coated with OPN and rinsed in Ca^{2+} buffer (Fig. 4 *a*). These conflicting results indicate that changes in the surface conformation of the adsorbed proteins, determined by the adsorption and buffer conditions and not resolved by our experiments, have a strong influence on the normal forces and adhesion between the surfaces.

SFA versus AFM

Our results show that the technique used to measure the forces, AFM (Figs. 1 and 2) or SFA (Figs. 3–5), is the most important factor in determining the shape of the force curves, and in particular the presence of adhesion. The geometry of the surfaces around the contact position can be approximated as a sphere of radius R in front of a plane for both AFM and SFA. However, the radius $R_{AFM} \approx 30$ nm is comparable to protein dimensions, whereas $R_{SFA} \approx 10^6 R_{AFM}$. The compliance of the cantilever and force sensitivity of the AFM is also ~5 orders of magnitude higher than that for SFA. Therefore, the AFM allows us to detect the forces generated by a few proteins, whereas SFA probes a much larger area of the surface and averages the normal forces generated by a distribution of protein conformations. For example, the sequence of sharp discontinuities observed in AFM force measurement (Fig. 1) are due to the breaking of single sacrificial bonds during retraction. Conversely, the SFA force curve is continuous because small fluctuations in the force due to small groups of proteins are negligible compared to the average force generated by the ensemble of the proteins confined between the macroscopic SFA surfaces.

Attractive forces appear in the SFA as a single, shallow minimum (Figs. 4 *a* and 5, *c* and *d*) from which the surfaces jump out at a distance D such that $d(F/R)/dD = K/R$ (see Figs. 4 *a* and 5, *c* and *d*). The starting and ending points of the jump-out will be located along a straight line of slope K/R connecting two stable regions of the force curve (i.e., where $d(F/R)/dD < K/R$) (36). Even if multiple minima were present in the retraction force curve, these could be detected only if the force wells around these minima were intersected by the straight line of slope K/R starting from the primary minimum. When attraction was consistently measured in SFA force measurements in the presence of calcium (Fig. 5, *c* and *d*), the distance $L_{SFA} = 10$–20 nm between the point where the force first became zero upon retraction and the starting point of the jump-out was of the same order of magnitude as the average value of the pulling length, $L = 60$ nm, measured by AFM on the same surface (Fig. 2 *b*). Both L_{SFA} and L are smaller than the contour length $l_c \approx 100$ nm of the protein, showing that the average length of the protein portion that forms cross-layer bridges and creates attraction between the surfaces is smaller than l_c. However, AFM force measurements occasionally show values of $L > l_c$, which are due to aggregation of the proteins. These events constitute a fraction of the protein population too small to produce a force detectable by the SFA.

Factors that complicate the comparison between AFM and SFA results are the pressure and the loading-unloading rate. In SFA measurements (Figs. 3–5), when the force reached the maximum value F_p upon compression (preload), the pressure at the center of the contact region was (37): $P_{SFA} = (-1/2\pi)\, d(F/R)/dD = 1$–$10$ atm. In AFM experiments, we chose the preload $F_p = 500$ pN (Fig. 1) to obtain a comparable pressure, $P_{AFM} = F_p/A \approx 2$ atm, considering a contact area $A = \pi R^2_{AFM}$. However, the AFM technique does not allow us to directly measure A or to determine the degree of indentation of the tip in the surface layer during compression; this leads to an unavoidable uncertainty: P_{AFM} must be considered a lower bound. Moreover, in SFA experiments, pressure increased at an average rate of 10^{-3}–10^{-2} atm/s, which is much slower than the AFM rate of 1–10 atm/s. Therefore, SFA measurements reflect a situation that is closer to equilibrium than in AFM. The relevance of this aspect will be investigated in further experiments.

Osteopontin as an adhesive in human bones

Fig. 6 shows that there is a particular adsorption geometry for which OPN produces a large adhesion between the two mica surfaces of the SFA. OPN was adsorbed from the OPN/Ca^{2+} solution at the edge of the circular contact area between two adhering bare mica surfaces (Fig. 6, *inset a*). When the surfaces are separated for the first time after adsorption, we measured an adhesion F_m that is almost five times stronger than the adhesion between mica surfaces in pure, OPN-free Ca^{2+} buffer. Under these adsorption conditions, OPN forms protein bridges between the two mica surfaces at the edge of the contact area, all of which have to be completely broken to retract the surfaces (Fig. 6, *inset b* and *c*). The strong adhesion is due to a strong OPN-mica binding or to a large density of bridges that is never reached during SFA experiments with precoated mica surfaces. The fact that upon retraction the surfaces stay at the same distance $D_m < 1$ nm before directly jumping out to large distances indicates that all protein bridges have already been broken when the mica-mica junction separates (Fig. 6 *c*). After complete separation of the surfaces, OPN started adsorbing on the area left uncoated during contact (Fig. 6, *inset d*). Before the adsorption reached equilibrium, the surfaces were brought into contact again (Fig. 6, *inset e*). This forced the proteins to flatten on mica, creating both protein bridges and intralayer surface-protein bonds. The force measured upon the second retraction after a short dwelling time in contact is less adhesive than for the first retraction, most likely because fewer protein bridges were created during the second approach than during the initial adsorption. The final force after 16 h and seven approach/retraction cycles was purely repulsive, like the one between two precoated mica surfaces (Figs. 4, *a* and *b*, and 5, *a* and *b*), but the surface coverage is below the detection limit, $\Gamma < 1$ mg/mm^2 (Table 2), and the range of the repulsion is of a few nanometers (Fig. 6) instead of several tens of nanometers. Adsorbed proteins were trapped in a nonequilibrium flattened configuration (Fig. 6, *insets e* and *f*), where long portions of the protein are immobilized on the mica surface by long-lived Ca^{2+}-mediated bonds (19). Short unabsorbed portions of the protein are strongly end-anchored to the surface, and OPN can form only short protein bridges between the surfaces. Most likely, this creates a short-ranged negative force during retraction, increasing with the distance more rapidly than the spring stiffness K and leading to the observed single jump-out (Fig. 6).

The behavior described in Fig. 6 is similar to what was observed for another protein with proposed adhesive properties, mussel foot protein (MFP) (12), which mediates the adhesion of mussels to rocks in salty sea water. Two mica surfaces precoated with MFP do not adhere to each other, because almost all surface-active residues are strongly attached to the substrate and become hidden from the other mica surface by a layer of nonbinding residues. Strong adhesion is measured when MFPs are allowed to simultaneously bind to both mica surfaces, as done for OPN in Fig. 6. In addition, it is possible to activate the adhesive potential of some MFPs by shearing the preadsorbed layer against an uncoated surface, which brings some of the surface-active residues to the shearing surface. A similar mechanism may contribute to the large adhesion observed by AFM on preadsorbed layers of OPN. During an AFM pulling experiment the tip is lowered onto the sample and a fixed preload is pressed into it. This results in a shearing motion of the cantilever parallel to the surface and produces a plowing out of the surface-active residues.

Finally, in view of the SFA results presented in Fig. 6, we suggest that OPN may act as an effective adhesive within bone (5) if it is allowed to simultaneously bind to two or more mineralized collagen fibrils separated by a few nanometers (1). The adhesion could also be increased by the particular physical-chemical composition of the hydroxyapatite nanocrystals coating the fibrils, which is different from that of mica, and by specific OPN-hydroxyapatite interactions. The latter are not well understood and are documented only to a small extent; there exists a report demonstrating the ability of OPN to influence the growth of calcium monooxalate crystals, the main mineral found in kidney stones (38). In this system the influence of OPN varies on specific lattice planes of the crystal, which further suggests that the adhesive or repulsive properties of OPN deposits depend strongly on the substrate.

CONCLUSIONS

Our combined AFM and SFA force measurements reveal that layers of OPN adsorbed on mica have interesting mechanical properties, which come from nonequilibrium molecular adsorption and cross-linking mechanisms triggered or enhanced by the presence of calcium ions. In particular, OPN layers have a inelastic behavior due to their ability to store energy in the form of long-lived calcium salt bridges, probably with the underlying mica surface. Interestingly, OPN is

not a generically good adhesive between mica surfaces; OPN layers in contact over a large area do not necessarily adhere to each other. Adhesion generally appears at the short length scale probed by the AFM and at the macroscopic scale only when OPN is allowed to bind to both surfaces at the same time—a condition that may be satisfied between mineralized collagen fibers of the bone.

We thank Dr. Larry W. Fisher at the National Institute of Dental and Craniofacial Research and Skeletal Diseases (National Institutes of Health, Department of Health and Human Services) in Bethesda, MD, for providing purified osteopontin and for helpful discussions. We thank Prof. Jacob Israelachvili at the Materials Department of the University of California at Santa Barbara for the use of the SFA and for useful comments on the manuscript.

P.K.H. acknowledges financial support from the National Institutes of Health, grant No. RO1 GM065354.

REFERENCES

1. Weiner, S., and H. D. Wagner. 1998. The material bone: structure mechanical function relations. *Annu. Rev. Mater. Sci.* 28:271–298.
2. Fantner, G. E., T. Hassenkam, J. H. Kindt, J. C. Weaver, H. Birkedal, L. Pechenik, J. A. Cutroni, G. A. G. Cidade, G. D. Stucky, D. E. Morse, and P. K. Hansma. 2005. Sacrificial bonds and hidden length dissipate energy as mineralized fibrils separate during bone fracture. *Nat. Mater.* 4:612–616.
3. Gupta, H. S., J. Seto, W. Wagermaier, P. Zaslansky, P. Boesecke, and P. Fratzl. 2006. Cooperative deformation of mineral and collagen in bone at the nanoscale. *Proc. Natl. Acad. Sci. USA.* 103:17741–17746.
4. Thompson, J. B., J. H. Kindt, B. Drake, H. G. Hansma, D. E. Morse, and P. K. Hansma. 2001. Bone indentation recovery time correlates with bond reforming time. *Nature.* 414:773–775.
5. Fantner, G. E., J. Adams, P. Turner, P. J. Thurner, L. W. Fisher, and P. K. Hansma. 2007. Nanoscale ion mediated networks in bone: osteopontin can repeatedly dissipate large amounts of energy. *Nano Lett.* 7:2491–2498.
6. Gupta, H. S., P. Fratzl, M. Kerschnitzki, G. Benecke, W. Wagermaier, and H. O. Kirchner. 2007. Evidence for an elementary process in bone plasticity with an activation enthalpy of 1 eV. *J. R. Soc. Interface.* 4:277–282.
7. Fisher, L. W., D. A. Torchia, B. Fohr, M. F. Young, and N. S. Fedarko. 2001. Flexible structures of SIBLING proteins, bone sialoprotein, and osteopontin. *Biochem. Biophys. Res. Commun.* 280:460–465.
8. Blom, N., S. Gammeltoft, and S. Brunak. 1999. Sequence and structure-based prediction of eukaryotic protein phosphorylation sites. *J. Mol. Biol.* 294:1351–1362.
9. Safran, J. B., W. T. Butler, and M. C. Farach-Carson. 1998. Modulation of osteopontin post-translational state by 1, 25-(OH)2-vitamin D3. Dependence on Ca^{2+} influx. *J. Biol. Chem.* 273:29935–29941.
10. Chen, Y., B. S. Bal, and J. P. Gorski. 1992. Calcium and collagen binding properties of osteopontin, bone sialoprotein, and bone acidic glycoprotein-75 from bone. *J. Biol. Chem.* 267:24871–24878.
11. Fantner, G. E., E. Oroudjev, G. Schitter, L. S. Golde, P. Thurner, M. M. Finch, P. Turner, T. Gutsmann, D. E. Morse, H. Hansma, and P. K. Hansma. 2006. Sacrificial bonds and hidden length: unraveling molecular mesostructures in tough materials. *Biophys. J.* 90:1411–1418.
12. Lin, Q., D. Gourdon, C. Sun, N. Holten-Andersen, T. H. Anderson, J. H. Waite, and J. N. Israelachvili. 2007. Adhesion mechanism of the mussel foot proteins mfp-1 and mfp-3. *Proc. Natl. Acad. Sci. USA.* 104:3782–3786.
13. Fedarko, N. S., B. Fohr, P. G. Robey, M. F. Young, and L. W. Fisher. 2000. Factor H binding to bone sialoprotein and osteopontin enables tumor cell evasion of complement-mediated attack. *J. Biol. Chem.* 275:16666–16672.
14. Israelachvili, J. N., and P. M. McGuiggan. 1990. Adhesion and short-range forces between surfaces. Part I: New apparatus for surface force measurements. *J. Mater. Res.* 5:2223–2231.
15. Israelachvili, J. N. 1973. Thin film studies using multiple-beam interferometry. *J. Colloid Interface Sci.* 44:259–272.
16. Israelachvili, J. N. 1991. Intermolecular and Surface Forces. Academic Press, London.
17. Ball, V., and J. J. Ramsden. 1998. Buffer dependence of refractive index increments of protein solutions. *Biopolymers.* 46:489–492.
18. Voros, J. 2004. The density and refractive index of adsorbing protein layers. *Biophys. J.* 87:553–561.
19. Luckham, P. F., and J. Klein. 1984. Forces between mica surfaces bearing adsorbed polyelectrolyte, poly-L-lysine, in aqueous media. *J. Chem. Soc., Faraday Trans. 1.* 80:865–878.
20. Raviv, U., J. Frey, R. Sak, P. Laurat, R. Tadmor, and J. Klein. 2002. Properties and interactions of physigrafted end-functionalized poly (ethylene glycol) layers. *Langmuir.* 18:7482–7495.
21. Tadmor, R., N. H. Chen, and J. N. Israelachvili. 2002. Thin film rheology and lubricity of hyaluronic acid solutions at a normal physiological concentration. *J. Biomed. Mater. Res.* 61:514–523.
22. Gaines, G. L. 1956. Surface adhesion and elastic properties of mica. *Nature.* 178:1304–1305.
23. Perez, E., and J. E. Proust. 1987. Forces between mica surfaces covered with adsorbed mucin across aqueous solution. *J. Colloid Interface Sci.* 118:182–191.
24. Kamiyama, Y., and J. Israelachvili. 1992. Effect of pH and salt on the adsorption and interactions of an amphoteric polyelectrolyte. *Macromolecules.* 25:5081–5088.
25. Malmsten, M., E. Blomberg, P. Claesson, I. Carlstedt, and I. Ljusegren. 1992. Mucin layers on hydrophobic surfaces studied with ellipsometry and surface force measurements. *J. Colloid Interface Sci.* 151:579–590.
26. Zappone, B., M. Ruths, G. W. Greene, G. D. Jay, and J. N. Israelachvili. 2007. Adsorption, lubrication, and wear of lubricin on model surfaces: polymer brush-like behavior of a glycoprotein. *Biophys. J.* 92:1693–1708.
27. Claesson, P. M., E. Poptoshev, E. Blomberg, and A. Dedinaite. 2005. Polyelectrolyte-mediated surface interactions. *Adv. Colloid Interface Sci.* 114:173–187.
28. Flory, P. J. 1969. Statistical Mechanics of Chain Molecules. Cornell University Press, Ithaca, NY.
29. Pashley, R. M. 1981. DLVO and hydration forces between mica surfaces in Li^+, Na^+, K^+, and Cs^+ electrolyte solutions: a correlation of double-layer and hydration forces with surface cation exchange properties. *J. Colloid Interface Sci.* 83:531–546.
30. Leckband, D., and J. Israelachvili. 2001. Intermolecular forces in biology. *Q. Rev. Biophys.* 34:105–267.
31. Claesson, P. M., P. Herder, P. Stenius, J. C. Eriksson, and R. M. Pashley. 1986. An ESCA and AES study of ion-exchange on the basal plane of mica. *J. Colloid Interface Sci.* 109:31–39.
32. Julenius, K. 2007. NetCGlyc 1.0: prediction of mammalian C-mannosylation sites. *Glycobiology.* 17:868–876.
33. Julenius, K., A. Molgaard, R. Gupta, and S. Brunak. 2005. Prediction, conservation analysis, and structural characterization of mammalian mucin-type O-glycosylation sites. *Glycobiology.* 15:153–164.
34. Reference deleted in proof.
35. Johansen, M. B., L. Kiemer, and S. Brunak. 2006. Analysis and prediction of mammalian protein glycation. *Glycobiology.* 16:844–853.
36. Landman, U., W. D. Luedtke, N. A. Burnham, and R. J. Colton. 1990. Atomistic mechanisms and dynamics of adhesion, nanoindentation, and fracture. *Science.* 248:454–461.
37. Klein, J., E. Kumacheva, D. Mahalu, D. Perahia, and L. J. Fetters. 1994. Reduction of frictional forces between solid surfaces bearing polymer brushes. *Nature.* 370:634–636.
38. Qiu, S. R., A. Wierzbicki, C. A. Orme, A. M. Cody, J. R. Hoyer, G. H. Nancollas, S. Zepeda, and J. J. De Yoreo. 2004. Molecular modulation of calcium oxalate crystallization by osteopontin and citrate. *Proc. Natl. Acad. Sci. USA.* 101:1811–1815.
39. Monigatti, F., E. Gasteiger, A. Bairoch, and E. Jung. 2002. The sulfinator: predicting tyrosine sulfation sites in protein sequences. *Bioinformatics.* 18:769–770.